

1

2 Performance of physically and chemically

3 activated biochars in copper removal from

4 contaminated mine effluents

5

6

7

8

9 Flavia Lega Braghiroli^{1,2}, Hassine Bouafif², Carmen Mihaela

10 Neculita³, Ahmed Koubaa¹

11

12

13 ¹ Research Forest Institute (Institut de recherche sur les forêts - IRF), University of Québec in

14 Abitibi-Témiscamingue (UQAT), 445 Boul. de l'Université, Rouyn-Noranda, QC J9X 5E4,

15 Canada

16 ² Centre Technologique des Résidus Industriels (CTRI, Technology Center for Industrial

17 Waste), Cégep de l'Abitibi-Témiscamingue (College of Abitibi-Témiscamingue), 425 Boul. du

18 Collège, Rouyn-Noranda, QC J9X 5E5, Canada

19 ³ Research Institute on Mines and Environment (RIME), University of Québec in Abitibi-

20 Témiscamingue (UQAT), 445 Boul. de l'Université, Rouyn-Noranda, QC J9X 5E4, Canada

25 **Abstract**

26 The increasing global demand for metals and minerals justifies the intensive study of treatment
27 options for contaminated mine effluents. The present study evaluated the conversion of wood
28 residues into physically and chemically activated biochars, and their subsequent use in the
29 treatment of Cu in synthetic and actual contaminated mine drainage. First, wood residues were
30 converted into biochar by fast pyrolysis. Then, physical (using steam or CO₂) or chemical (using
31 KOH) activation was carried out in a homemade pilot-scale furnace. After activation, highly
32 microporous (KOH materials) and micro/mesoporous activated biochars (CO₂ and steam
33 materials) were obtained. Batch adsorption testing was first conducted with synthetic effluents.
34 Results showed that CO₂-activated biochar was the most Cu effective adsorbent (99% removal)
35 at low concentrations (5–20 mg L⁻¹). The mechanisms of Cu²⁺ adsorption involved physical and
36 chemisorption for biochars and CO₂-activated biochar, while chemisorption for KOH-activated
37 biochars was probably due to the high proportion of functional groups connected to their
38 surface. In multi-metal acid mine drainage, metal adsorption capacities deteriorated for most of
39 the materials, probably due to effects of ion competition. However, KOH-activated biochar
40 decreased Cu²⁺ concentrations to below the authorized monthly mean allowed by Canadian law
41 (0.3 mg L⁻¹), and decreased Co, Pb, and Mn concentrations up to 95%. These findings indicate
42 that high porosity and oxygenated functional groups connected to the surface of activated
43 biochars are important properties for the enhancement of interactions between carbon materials
44 and metals from mine effluents, as well as for their performance improvement in mine drainage
45 treatment.

46

47

48 **Keywords:** Activated biochar, adsorption, copper removal, water treatment, actual mine
49 effluents

50 **1. Introduction**

51 Current mining activities, which exploit low-grade ore, generate large amounts of waste.
52 The subsequent contamination is associated with air pollution by gases (CO₂, SO₂, NO_x, etc.)
53 and particulate matter emissions, solid waste that deteriorates the soil, and contaminated
54 effluents that may reach drinking water systems and pose a risk to humans and wildlife (Dudka
55 and Adriano 1997). The main issue is the exposure of geochemically reactive minerals to air
56 and water, which leads to contaminated mine drainage, either acidic (AMD) or contaminated
57 neutral (CND), as well as to surface and underground water pollution (Nordstrom et al. 2015).
58 Cu mining and smelting are one of the major sources of mine waste. Although Cu is an essential
59 element required for living organisms, its divalent form (Cu²⁺) is potentially toxic and
60 carcinogenic when ingested by aquatic organisms and humans. An excess of Cu leads to
61 vomiting, headache, nausea, liver/kidney failure, and respiratory problems (Akar et al. 2009),
62 and can be harmful to soil biota, plants (Lamb et al. 2012), and aquatic ecosystems (Lee et al.
63 2010).

64 Several regulators monitor the levels of Cu in wastewater treatment plants, drinking water,
65 and industrial effluents to certify that the maximum contaminant level should be below a value
66 at which there is no known or expected risk to health. In drinking water, Health Canada fixed
67 the threshold at less than 1 mg L⁻¹ (Health Canada 1992), whereas the maximum authorized
68 monthly mean concentration of Cu should be below 0.3 mg L⁻¹ according to metal mining
69 effluent regulations (Environment and Climate Change Canada 1999). Several options are
70 available for the treatment of Cu in water: chemical precipitation, ion exchange, membrane
71 filtration, coagulation/flocculation, electrolytic recovery, reverse osmosis, and adsorption. Each
72 technology has its advantages and limits for an efficient Cu removal from wastewater, but high
73 costs are a common drawback. However, adsorption is an attractive technique due to the
74 availability of cost-effective, sustainable, and eco-friendly bioadsorbents (Sekhula et al. 2012).

75 Literature reveals that activated carbons are the most appropriate bioadsorbents between algal,
76 bacterial, agriculture and forest, and fungal and yeast biomass for Cu uptake in water media
77 (Bilal et al. 2013).

78 Several inexpensive waste precursors have been used for the production of activated
79 carbons, including wood residues, fruit shells, stones, husks, and hulls (Tan et al. 2017).
80 Recently, biochar, a by-product carbon-rich material produced from the thermochemical
81 conversion processes of biomass (e.g., torrefaction, slow to fast pyrolysis, and gasification) has
82 also been tested (Lehmann and Joseph 2015). Although biochar has high carbon content and a
83 high proportion of oxygenated functional groups, it is often characterized by low surface area
84 with a small amount of micropores (Liu et al. 2015). Activation is a widely used technique in
85 which a selective gasification of carbon atoms by physical agents (CO₂ or steam) or chemicals
86 (KOH or H₃PO₄) is performed at increasing temperature (e.g., 900 °C) for the development of
87 materials' porosity (Marsh and Rodríguez-Reinoso 2006). The feedstock, pyro-gasification, and
88 activation operating conditions have significant influence on the resultant activated biochar,
89 while highly porous materials with properties similar to activated carbons (e.g., surface areas
90 up to 2500 m² g⁻¹) can be produced. However, an optimization study of the operating conditions
91 for the preparation of activated biochars to improve the material porosity is required (Braghiroli
92 et al. 2018a).

93 The effective sorption of metals by activated biochars made by using different operating
94 conditions and feedstock have been reported in the literature. According to a very recent review
95 (Braghiroli et al. 2018b), the surface functional groups (e.g., carboxylic, phenolic, amino
96 groups), specific surface area, and pore volume (narrow and wide micropores), as well as the
97 optimum pH, are the most important factors in potentially providing more bonding sites for
98 heavy metals interactions with activated biochars. The overall metal removal mechanisms
99 include physical adsorption, electrostatic attraction between positive charges (metals) and

100 negative charges (surface of activated biochar), ion exchange, surface complexation, and metal
101 precipitation (Chowdhury et al. 2012; Adebisi et al. 2017a, 2017b). Hence, the removal of up
102 to 18 mg g⁻¹ of Cu (C₀ from 50 to 100 mg L⁻¹) was reported using KOH-activated fruit peel of
103 mangostene biochar (Hamid et al. 2014). Then, up to 96% of Cu (C₀ = 63.5 mg L⁻¹) elimination
104 using steam-activated soybean straw biochars was published by Lima et al. (2010). The
105 improved efficiency compared to biochars (96 vs. 85%) was associated with increased surface
106 area (up to 793 m² g⁻¹), which eventually facilitated the access of functional groups connected
107 to the surface of activated biochars. High adsorption capacity of Cu (203 mg g⁻¹; C₀ from 0.1 to
108 600 mg L⁻¹) was also attributed to the presence of both carboxylic and phenolic groups on steam-
109 activated date pit biochars, improving cation exchange and complexation of adsorbent surface-
110 metal interactions, as well as greater surface area (1467 m² g⁻¹) for physical sorption (Bouchelta
111 et al. 2012). In another study, steam-activated manure biochar showed high Cu sorption capacity
112 (104 mg g⁻¹; C₀ = 1270 mg L⁻¹) due to the presence of inorganics (e.g., P, S, Ca, Na) that played
113 an important role in the development of specific surface functionalities and of multiple
114 interactions between activated biochar' surface and Cu²⁺ ions. It was also reported that metals
115 sorption were favored at low pH level (fixed at 4.8), whereas at pH higher than 6, Cu
116 precipitation occurred (Lima et al. 2014).

117 Based on the authors' best knowledge, this study is the first to examine the use of wood
118 residues (white birch and black spruce) for the production of activated biochars in pilot-scale
119 technologies for the treatment of Cu in synthetic and actual mine effluents. Most previous
120 studies evaluated the performance of activated biochars in the removal of very high
121 concentrations of Cu from synthetic solutions, but very few studies focused on the use of
122 activated biochar for the removal of multi-metal contaminants from actual mine effluents.
123 According to the circular economy principle (recover and recycle, instead of "take, make, and
124 discard"), the use of wood residues in mine effluent treatment appears to be a winning formula

125 for both the mining and forestry industries, such as in Abitibi-Témiscamingue, the region of
126 Québec, Canada, where the present study was conducted.

127 In this context, the objective of the present study is to evaluate the removal efficiency of
128 physically and chemically activated biochars made from wood residues for the treatment of Cu
129 in synthetic effluent and actual AMD.

130

131 **2. Materials and methods**

132 2.1 Material sampling and synthesis of biochar and activated biochar

133 White birch (WB) and black spruce (BS) residues were sampled from sawmills located in
134 the Abitibi-Témiscamingue region, Québec, Canada. More details on wood residues
135 preparation, CarbonFX fast pyrolysis technology, and pilot-scale activation furnace are
136 available elsewhere (Braghiroli et al. 2018a). In summary, biochars were produced at 454 °C in
137 an oxygen-free environment using the CarbonFX fast pyrolysis technology developed by Airex
138 Energy Inc. (Bécancour, QC, Canada). The resulting biochars made from WB and BS residues
139 were activated in a homemade pilot oven. Three types of activating agents were used for the
140 production of activated biochars: KOH, CO₂, and steam. In chemical activation, 100 g of each
141 biochar were mixed with 200 g of distilled water and 100 g of KOH, and left in the fume hood
142 for 2 h. Then, the mixture was left in an oven at 120 °C overnight. The impregnated biochar
143 was then placed in the feed hopper; and when the furnace reached 900 °C in a N₂ atmosphere,
144 the material was transported into the furnace by a screw conveyor (driven by an electronic
145 engine) to the recovery hopper. The same procedure was carried out in physical activation, in
146 which the flowing gas of CO₂ (3 L min⁻¹) or steam (0.3 L min⁻¹) was introduced when the
147 temperature reached 900 °C. The raw biochars were labelled BWB and BBS, while activated

148 biochars depending on the type of activation agent, were labelled as e.g., CO2BWB, KOHBWB,
149 or H2OBBS.

150 2.2 Physical and chemical characterization of biochar and activated biochar

151 Biochars and activated biochars were characterized for their physicochemical parameters:
152 pH, elemental composition (C, H, N, S, O), morphology, surface chemistry, specific surface
153 area, and pore volume. The pH of activated biochars was determined according to a standard
154 test method (ASTM D3838 - 05(2017)) using a SevenMulti, Mettler Toledo (Greifensee,
155 Switzerland) equipped with Inlab Routine Pro electrode. Elemental composition of all materials
156 was determined in a CHNS elemental analyzer, Perkin Elmer 2400 CHNS/O Analyzer
157 (Waltham, MA, USA), by combustion of the samples in a stream of pure O₂. The morphology
158 of biochars and activated biochars was investigated with a JEOL JSM-5500 (JEOL USA, Inc.,
159 Peabody, MA, USA) Scanning Electron Microscope (SEM), after metallization. X-ray
160 photoelectron spectroscopy (XPS) spectra were recorded with a Kratos AXIS ULTRA system
161 (Wharfside, MA, UK) equipped with a channel electron multiplier detector. The XPS core level
162 spectra were analyzed with Casa software.

163 Micromeritics ASAP 2460 automatic apparatus (Norcross, GA, USA) was used for
164 obtaining N₂ adsorption/desorption isotherms of porous materials at -196 °C. The data were
165 then treated for measuring surface area, S_{BET} (m² g⁻¹), calculated by the Brunauer-Emmett-Teller
166 (BET) model (Brunauer et al. 1938); micropore volume, V_{μ, N_2} (cm³ g⁻¹), determined by the
167 Dubinin–Radushkevich (DR) equation (Dubinin 1989); total pore volume, V_t (cm³ g⁻¹),
168 calculated from the amount of nitrogen adsorbed at the relative pressure of 0.97 (Gregg and
169 Sing 1991); and mesopore volume, V_m (cm³ g⁻¹), calculated by the difference $V_t - V_{\mu, \text{N}_2}$.
170 Ultramicroporosity was obtained by CO₂ adsorption at 0 °C (V_{μ, CO_2} (cm³ g⁻¹)) and the pore size
171 distribution (PSD) was determined by application of density functional theory (DFT) using N₂
172 adsorption isotherms (Tarazona 1995).

173 2.3 Adsorption kinetics experiments

174 Kinetic experiments were conducted in 100 mL beakers containing 0.05 g of adsorbent
175 material and 50 mL of synthetic effluent with Cu^{2+} concentration of 100 mg L^{-1} . The
176 supernatants were sampled after predefined intervals at 2, 4, 6, 8, 10, 12, 18, 24, and 48 h. The
177 beakers were placed on a multi-position stirring plate, at 500 rpm, and at room temperature (20
178 ± 2 °C). The pH, potential redox (Eh), and dissolved oxygen (DO) of the supernatant were
179 measured in the beginning and on each sample collected. DO and Eh were measured using LDO
180 Hatch and ORP Hach (London, ON, Canada) meters, respectively, with a double junction
181 Ag/AgCl reference electrode. The supernatants were filtered, and the residual metal trace was
182 determined by using microwave plasma atomic emission spectroscopy (MP-AES 4200, Agilent
183 Technologies, Mississauga, ON, Canada). This procedure was carried out for all 8 materials,
184 including 2 biochars (BWB and BBS) and 6 activated biochars (CO2BWB, KOHBWB,
185 H2OBWB, CO2BSB, KOHBSB, and H2OBSB).

186 Sorption capacity q_t (mg g^{-1}) was calculated with the application of Eq. 1:

$$187 \quad q_t = [C_0 - C_t] \cdot \frac{V}{m} \quad (1)$$

188 where C_0 , C_t , V , and m represent, respectively, the concentrations of Cu in solution (mg L^{-1}) at
189 the initial and at t moment, the total volume of solution (L), and the amount of the material used
190 (g).

191 The equations of pseudo-first (Eq. 2) and pseudo-second (Eq. 3) order model (Lagergren
192 1898), and Elovich (Eq. 4) were employed to describe Cu adsorption kinetics.

$$193 \quad \log(q_e - q_t) = \log(q_e) - k_1 \cdot \frac{t}{2.303} \quad (2)$$

$$194 \quad \frac{1}{(q_e - q_t)} = \frac{1}{q_e} + k_2 t \quad (3)$$

$$195 \quad q_t = \frac{1}{b} \cdot \ln(ab) + \frac{1}{b} \cdot \ln(t) \quad (4)$$

196 where q_e and q_t refer to the amount of Cu adsorbed (mg g^{-1}) at equilibrium and at any time, t
 197 (h), respectively, and k_1 is the equilibrium rate constant of pseudo-second order adsorption (h^{-1})
 198 1), and k_2 is the kinetic constant of pseudo-first order adsorption (g (mg h)^{-1}), a is the initial
 199 adsorption rate (mg (g h)^{-1}), and the parameter $1/b$ is related to the number of sites available for
 200 adsorption.

201 2.4 Adsorption equilibrium experiments

202 The tests of isotherm adsorption were conducted at different initial Cu concentrations (5,
 203 10, 20, 50, 100, 200, 500, and 1000 mg L^{-1}) under the same conditions as the kinetic
 204 experiments. Equilibrium was carried out for 48 h adsorption testing. Sorption capacity q_e (mg
 205 g^{-1}) was calculated with Eq. 5, where C_0 , C_e , V , and m represent, respectively, the concentrations
 206 of Cu (mg L^{-1}) at the initial and equilibrium solutions, the total volume of solution (L), and the
 207 amount of the material used (g). The adsorption (%) was calculated with Eq. 6:

$$208 \quad q_e = [C_0 - C_e] \cdot \frac{V}{m} \quad (5)$$

$$209 \quad \text{Adsorption (\%)} = [C_0 - C_e] \cdot \frac{100}{C_0} \quad (6)$$

210 The equations of Langmuir (Langmuir 1918) and Freundlich (Freundlich 1906) represented
 211 by Eq. 7 and 8, respectively, were employed to describe Cu sorption:

$$212 \quad \frac{C_e}{q_e} = \frac{1}{b \cdot q_{max}} + \frac{C_e}{q_{max}} \quad (7)$$

$$213 \quad \log q_e = \log k_f + n \cdot \log C_e \quad (8)$$

214 where C_e and q_e have the same meaning for both equations, q_{max} is the maximum uptake per
 215 unit mass of adsorbent (mg g^{-1}), and b is the Langmuir constant related to the adsorption energy
 216 (L mg^{-1}) while k_f and n are Freundlich coefficients.

217 The constant b allows the determination of the R_L equilibrium parameter (Eq. 9) that
 218 indicates the shape of the isotherm (at $R_L = 0$, the adsorption is irreversible; $0 < R_L < 1$, the

219 adsorption is favorable; at $R_L = 1$, the adsorption is linear; and at $R_L > 1$, the adsorption is
220 unfavorable):

$$221 \quad R_L = \frac{1}{1 + b \cdot C_0} \quad (9)$$

222 2.5 Adsorption of Cu in actual mine effluent

223 The actual effluent, containing Cu and other metals, was collected from an operating gold
224 mine located in Abitibi-Témiscamingue, QC, Canada, and preserved at 4 °C, prior to testing.
225 The same testing conditions for the kinetics and isotherms studies of Cu in synthetic effluents
226 were also applied for this effluent. The supernatants were filtered, and the residual metals were
227 measured by MP-AES equipment while the pH, Eh, and DO were measured using the same
228 multimeter. Anions (NO_2^- , NO_3^- , SO_4^{2-} , PO_4^{3-}) were determined using the ion chromatography
229 Dionex ICS-5000 with a capillary column Ionpac AS18 (ThermoFisher Scientific, Waltham,
230 USA).

231 2.6 Geochemical modelling

232 The thermodynamic geochemical equilibrium model Visual MINTEQ (VMINTEQ)
233 version 3.1 (Visual MINTEQ 2018) was applied to calculate saturation indices (SI) of potential
234 mineral phases present in the AMD. The data on the effluent (e.g., pH, contaminant
235 concentrations) was used to calculate equilibrium distribution of chemical species according to
236 geochemical processes (e.g., precipitation, complexation, ion exchange). If $\text{SI} < 0$, minerals are
237 undersaturated or in a dissolved form; if $\text{SI} = 0$, minerals are at equilibrium; and finally if $\text{SI} >$
238 0, minerals are oversaturated and might precipitate.

239 2.7 Activated biochar regeneration

240 Chemical regeneration tests were performed with an activated biochar for six cycle
241 adsorption-desorption tests. Adsorption tests were conducted under the same conditions as the
242 isotherm experiments. After sorption, 0.1 g of dried adsorbent was mixed and shaken with 20

243 mL eluents of 0.1 M HNO₃, 0.5 M H₂SO₄, and 1 M HCl, according to Kołodyńska et al. (2017).
244 The desorption was determined using Eq. 10:

$$245 \quad \%D = \frac{C_{des}}{C_0} \times 100\% \quad (10)$$

246 where C_0 and C_{des} (mg L⁻¹) are the initial Cu concentration and the concentration of Cu ions in
247 solution after desorption, respectively.

248

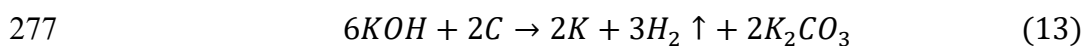
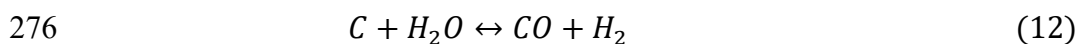
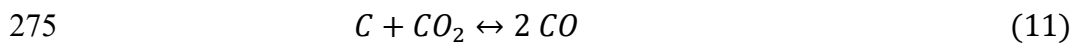
249 **3. Results and discussion**

250 **3.1 Physicochemical characterization of the activated biochars**

251 SEM images of activated biochars (Fig. 1) show a typical morphology of wood-derived
252 carbons where the original wood structure is maintained. Fast pyrolysis followed by activation
253 leads to the formation of various sizes of pits, holes, and cave-type openings on the carbon
254 structure for all three types of activating agents. The development of narrow and wide pores
255 was noticed, but no clear structural differences were identified across materials physically or
256 chemically activated. The physicochemical properties of biochar and activated biochars are
257 presented in Table 1. Notably, the carbon content of materials made by fast pyrolysis and
258 activation substantially increased, whereas oxygen and hydrogen contents decreased. During
259 the thermal treatment of lignocellulosic and biochar-derived materials, various carbon
260 compounds (e.g., H₂O, CO₂, CO, NH₃, HCN, C_xH_yO_z) are released. With further increase in
261 temperature, compounds with less carbon (e.g., CO₂, CO, NO_x) are continuously released,
262 leading to increased material's carbon content and pore development (Liu et al. 2015).

263 Biochar activation involves mostly a reaction between the carbon (in biochar molecular
264 structure) and injected CO₂ or steam as seen in Eq. 11 (Boudouard reaction) (Calo and Perkins
265 1987) and Eq. 12, respectively. In fact, the physical agents will promote the removal of carbon
266 atoms (burn off) from the structure of biochar at high temperatures, causing the development of

267 pores. In chemical activation, the main reaction mechanism (Eq. 13), as proposed by Radovic
268 and Rodriguez-Reinoso (1997), involves the following steps: KOH dehydration to form K₂O;
269 K₂O reduction to metallic potassium (K); K oxidation to form K₂O; and K₂O hydration to form
270 KOH. Chemical activation is considered efficient because different potassium compounds and
271 gases (physical agents) are formed as well as K that penetrates into the biochar structure to
272 expand its framework and porosity. Therefore, before and after activation, materials showed an
273 acid and basic character, respectively. At any type of activation, pH ranged from 8.2 to 10.3
274 (Table 1).



278 The oxygen functional groups present on the surface of biochars and activated biochars were
279 investigated by XPS. After deconvolution of C1s peaks, the relative proportions of the
280 functional groups were estimated (Supplementary Material, Table 1S). The two most
281 predominant peaks measured for most of all materials were related to aliphatic/aromatic carbon
282 (C–C, C–H, and C=C), at BE lower than 285 eV (62–76%), and the C–O bond, at BE in a range
283 285.7–287.1 (18–8%). The other peaks (at 286.1–288, and 288–289.4 eV) were then attached
284 to the oxygen-containing moieties, i.e., C=O or O–C–O, and O–C=O, respectively (Lazzarini
285 et al. 2016). KOH-activated biochars had the highest proportion of total oxygenated groups:
286 22.4 and 25.4% for KOHBBS and KOHBWB, respectively, followed by CO2BWB (19.5%),
287 H2OBWB (17.9%), CO2BBS (17.5%), and H2OBBS (13.4%). In addition, KOHBBS had a
288 more evenly divided proportion of oxygenated groups—8.1% (C–O bond), 7.9% (C=O or
289 O–C–O), and 6.4% (O–C=O) relative to CO2BWB, 12.8, 4.5, and 2.2%, respectively—which
290 can have more distinct and abundant interactions with metals.

291 Analysis of the textural properties of biochars shows that they are highly ultramicroporous,
292 as evidenced by the CO₂ adsorption analysis with low surface areas: 177 and 208 m² g⁻¹ for
293 BWB and BBS, respectively. After activation, birch-activated biochars presented highly
294 developed surface areas in presence of KOH, CO₂, and steam, 1700, 881, and 590 and m² g⁻¹,
295 respectively. However, these materials had a porous structure highly different from each other.
296 According to the IUPAC classification (Sing 1985), N₂ adsorption/desorption isotherms at -196
297 °C for KOH-activated biochars are of Type I, characteristic of microporous solids with a narrow
298 elbow at $P/P_0 = 0.05$ and a horizontal plateau (Fig. 1S a). For the other materials, the N₂
299 isotherms are a combination of Type I and Type IV, with an important nitrogen uptake at relative
300 pressures $P/P_0 < 0.01$. This indicates the existence of a well-developed narrow microporosity,
301 and a slight slope up to $P/P_0 = 0.9$. The development of wider microporosity and mesoporosity
302 with the presence of a narrow hysteresis loop is hence confirmed. PSDs obtained by DFT (Fig.
303 1S b) are in good agreement with results obtained from N₂ isotherms. No pics higher than 2 nm
304 were observed for highly microporous KOH-activated biochars (i.e., 0% mesoporosity),
305 whereas the other materials presented two pics: one in micropore range (< 2 nm), and the other
306 in mesopores (10–50 nm).

307 3.2 Adsorption kinetics

308 The kinetics of adsorption describe the rate of Cu²⁺ ions uptake on biochar-derived
309 materials. The adsorption capacity of Cu²⁺ increased with time for all materials (Fig. 2). The
310 adsorption equilibrium was reached for most of materials at 24 h testing. Thereafter, it reached
311 a plateau, which indicates that no additional Cu²⁺ was removed from the synthetic effluent at
312 100 mg L⁻¹. The Cu²⁺ adsorption capacity for CO₂BWB increased 5 times (~49 mg L⁻¹)
313 compared to biochars (~10 mg L⁻¹). The adsorption capacities of biochar-derived materials for
314 Cu²⁺ varied according to the following sequence: CO₂BWB < KOHBBS < H₂O BWB <
315 KOHBWB ~ CO₂BBS < H₂O BBS < BBS ~ BWB.

316 The experimental data for the adsorption of Cu^{2+} onto biochar-derived materials were
317 interpreted with the kinetic models (pseudo-first and pseudo-second order, and Elovich's
318 equation) to evaluate the controlling mechanism of adsorption process. The derived kinetic
319 parameters of these models (Table 2) show that experimental data obtained from biochars and
320 activated biochars do not follow the pseudo-second kinetic model as evidenced by R^2
321 coefficients between 0.02 and 0.72. Biochars and CO_2 -activated biochars best fit the pseudo-
322 first ($R^2 = 0.79\text{--}0.99$) and Elovich models ($R^2 = 0.82\text{--}0.97$), whereas steam and KOH-activated
323 biochars best defined the adsorption process of the Elovich kinetic model as evidenced by R^2
324 coefficients: 0.67–0.95. These results are in agreement with several other metal adsorption
325 systems that have been described by the Elovich equation (Wu et al. 2009).

326 Pseudo-first model is based on the assumption that physisorption limits the rate of
327 adsorption of Cu^{2+} onto the adsorbent (Lagergren 1898), whereas the Elovich model gives a
328 good correlation on highly heterogeneous surfaces and chemisorptive interaction onto
329 materials' surface (Aharoni and Tompkins 1970). These results suggest that physical and
330 chemical interactions may simultaneously contribute and control Cu^{2+} uptake onto biochars and
331 CO_2 -activated biochars surfaces, whereas chemisorption is the main adsorption interaction
332 between Cu^{2+} metal ions and activated biochars made with steam and KOH. Physisorption
333 involves Van der Waals or electrostatic forces as confirmed by the effect of optimum pH (4.5),
334 while chemisorption involves covalent forces (Xie et al. 2017), which can be formed with active
335 oxygenated functional groups as observed by XPS analysis in the prepared materials structure
336 (Chowdhury et al. 2015).

337 3.3 Adsorption isotherms

338 Biochars and activated biochars were tested for their ability to adsorb Cu in synthetic
339 effluent. Comparative adsorption isotherms of Cu show that activated biochars (e.g., CO_2BWB)
340 exhibited almost fivefold higher Cu sorption relative to biochars (Fig. 3 a). The efficiency of

341 Cu removal in synthetic effluents ($C_0 = 5\text{--}20 \text{ mg L}^{-1}$) was up to 50%, for biochars, whereas it
342 varied from 95 to 99%, for activated biochars (Fig. 3 b). In addition, Cu removal for all materials
343 deteriorated with increases in initial concentrations. For example, CO2BWB decreased more
344 than four times (from 99 to 24%), when initial concentrations increased (from 5 to 200 mg L^{-1} ,
345 respectively).

346 Langmuir and Freundlich, two widely used isotherm models, were applied to describe the
347 sorption of Cu by biochars and activated biochars (Table 3). The Langmuir model describes the
348 monolayered adsorbents on the homogeneous surface (Langmuir 1918), whereas the Freundlich
349 model indicates that the adsorption would take place on a heterogeneous surface (Freundlich
350 1906). According to the correlation coefficients (R^2) listed in Table 3, the experimental data fit
351 Freundlich ($R^2 = 0.77\text{--}0.94$) better than Langmuir ($R^2 = 0.15\text{--}0.92$), although the separation
352 factor (R_L) lower than 1 suggests that Cu^{2+} adsorption on biochar-derived materials is a
353 favorable process. This result is consistent with the kinetic studies, in which data matched the
354 Elovich model, i.e., based on chemisorption process.

355 With an increase of Cu concentration to up to 1000 mg L^{-1} , KOHBBS showed the greatest
356 adsorption capacity: q_{exp} and q_{max} obtained from experiments and predicted based on Langmuir
357 model, respectively, were 137 and 132 mg g^{-1} . Ion exchange and complexation are the most
358 important mechanisms associated with Cu uptake by adsorbents (Baccar et al. 2009; Bouchelta
359 et al. 2012; Bilal et al. 2013). Hamid et al. (2014) reported that Cu was mainly adsorbed by
360 chemical interactions with active functional groups present on the surface of the KOH-activated
361 fruit peel of mangostene biochar. Indeed, KOHBBS presented a great and evenly divided
362 proportion of oxygenated groups (phenolic, carboxylic, aldehyde or ether), which improve the
363 cation exchange capacity and complexation properties of these adsorbents in addition to the
364 greater specific surface area and microporosity.

365 A comparison of adsorption capacity of Cu^{2+} on different activated biochars in the available
366 literature (Table 4) shows that higher adsorption capacities of activated biochar (even better
367 than commercial activated carbon) are attributed to several factors, as mentioned before, such
368 as physicochemical properties (high specific surface area, pore size, type of functional groups
369 connected to the materials surface), high affinity between carbon material and Cu^{2+} , optimum
370 pH, increasing carbon (g): contaminant (mL) ratio, and high initial Cu concentration used. The
371 comparable adsorption capacity of materials made in this study with other adsorbents reveals
372 that physical and chemical activated biochar made from wood residues is suitable for the
373 removal of Cu^{2+} since it has a relatively high adsorption capacity.

374 3.4 Cu removal in actual AMD

375 The initial concentration of Cu^{2+} in actual AMD (1.75 mg L^{-1}) collected from an operating
376 mine site largely exceeded the maximum authorized monthly mean concentration of Cu (0.3 mg
377 L^{-1}) allowed by the Canadian law (Environment and Climate Change Canada 1999). For most
378 of biochar-derived materials, the removal of Cu^{2+} was not significant, and varied from 17 to
379 56% (Fig. 4). The only material for which Cu removal topped 99% was KOHBBS. The sorption
380 of the activated biochar seems to be unaffected by the nature of the precursor (WB or BS).
381 Rather, it is associated with increased surface area (highly porous materials) and improved
382 access of functional groups connected to the surface of activated biochars that may have
383 improved the interactions between Cu and the surface of the material. KOHBBS also exhibited
384 the highest adsorption capacity in synthetic effluents at very high Cu concentrations.

385 Comparing the composition of AMD before and after adsorption onto KOHBBS (Table 5),
386 it was noticed that pH, Eh, and DO of the effluent did not vary significantly, but metal adsorption
387 capacities were reduced (Fig. 4) relative to single-metal synthetic effluent, probably due to
388 multi-metal competition from an actual effluent onto KOHBBS (Mohan and Chander 2001,
389 2006). In addition to Cu removal, other metals were also removed in presence of KOHBBS,

390 including Co, Fe, Mn, Na, Pb, and Zn (Table 5). Among these metals, Co and Pb had the highest
391 removal efficiency of 95 and 43%, respectively, although a significant increase of K is probably
392 coming from the KOH activation during the production of activated biochar. Therefore, a
393 decrease of metals concentration was observed in presence of activated biochar, even though a
394 pre- and/or post-treatment is required to reduce the level of metal concentrations (e.g., Mn, Zn,
395 Fe) to meet Canadian regulations (see q_{exp} in Table 3).

396 Metals can form soluble and precipitate complexes, but to precipitate them from water, the
397 pH must range from 6 to 9, although Fe^{3+} can precipitate at pH higher than 3.5 (Ríos et al. 2008).
398 According to VMINTEQ geochemical modelling, oversaturation and possible precipitation for
399 $MnHPO_4$ was performed in initial AMD, whereas all metals in AMD after sorption onto
400 KOHBBS were undersaturation. Ríos et al. (2008) employed a significant zeolite: effluent ratio
401 (5 g:100 mL) for the treatment of AMD, which increased the pH of the system, and,
402 consequently, metal concentrations decreased probably due to precipitation on the surface of
403 zeolite. According to Table 1, all materials, including KOHBBS, exhibited an acid character, so
404 precipitation of certain solid phases on the surface of the ion exchanger might not be promoted.
405 However, precipitation also depends on metal concentration, temperature, the existence of
406 metals and anions, and time to thermodynamic equilibrium (Cuppett 2006). In the study, at such
407 low adsorbent: effluent ratio (0.1 g:100 mL), the pH was maintained at very low value (2.6);
408 thus, the presence of a precipitate was not obvious.

409 3.5 Regeneration of activated biochar

410 The feasibility of the adsorption technology on an industrial scale depends on the
411 reusability of spent activated biochar. In addition, chemical regeneration is largely used for
412 desorbing inorganic contaminants, especially metals. Desorption experiments were carried out
413 in order to estimate the metal releasing capacity of an activated biochar loaded with Cu^{2+} . Three
414 types of acid eluents were applied for Cu desorption: HNO_3 , H_2SO_4 , and HCl at different

415 concentrations 0.1, 0.5, and 1 M. By comparing the three eluents, HNO₃ was found to be the
416 most efficient, even if used at the lowest concentration, followed by HCl and, finally, H₂SO₄.
417 Under strong acid condition, the surface of the sorbent is in a protonated form, which allows
418 desorption of positively charged ions. In the first adsorption-desorption cycle, desorption
419 efficiency was found to be 99.6, 99.2, and 98.6%, respectively (Fig 5. a). After the six
420 regeneration cycles (Fig. 5 b), the efficiency of Cu desorption was reduced to 76.2, 51.4, and
421 36.2% using HNO₃, H₂SO₄, and HCl, respectively. These results suggest that activated biochar
422 made from wood residues has high regenerability, more stable Cu desorption efficiency with
423 HNO₃ compared to the other two acid eluents, and suitability for a minimum of at least six
424 successive adsorption-desorption cycles.

425

426 4. Conclusion

427 Activated biochars were produced from wood residues using physical (steam and CO₂)
428 and chemical (KOH) processes. The experimental data revealed that Cu removal depends on
429 the physicochemical characteristics (e.g., high surface area and porosity, and oxygenated
430 functional groups connected to materials surface) of the sorbent material as well as the effluent
431 type (single or multi-metal) and initial metal concentrations ($C_0 < 2 \text{ mg L}^{-1}$ or $C_0 \geq 5 \text{ mg L}^{-1}$).
432 CO₂-activated biochar showed better efficiency for Cu in synthetic effluent at up to 200 mg L⁻¹,
433 whereas KOH-activated biochar was the most efficient material for Cu from high
434 concentration synthetic effluent (1000 mg L⁻¹) and from multi-metal actual effluent. Elovich
435 kinetic and Freundlich isotherm models were found to fit the experimental data, indicating that
436 chemical interactions of oxygenated functional groups with Cu on the heterogeneous surface
437 might be occurring. The desorption of Cu ions was successfully carried out through chemical
438 regeneration with HNO₃, which was the most efficient approach, even after six adsorption-
439 desorption cycles, relative to H₂SO₄ and HCl. Therefore, wood residues seem to be an attractive

440 precursor for the production of activated biochar for remediating Cu present in actual mine
441 effluent. However, a pre- and/or post-AMD treatment would be required to reduce high levels
442 of other metals such as Fe, Al, and Mn according to the fixed Canadian thresholds for mine
443 effluent.

444

445 **Acknowledgments**

446 This research was funded by the Québec's Ministry of Economy, Science and Innovation
447 (Ministère de l'Économie, de la Science et de l'Innovation du Québec), the Natural Sciences
448 and Engineering Research Council of Canada (NSERC), the Canada Research Chairs Program,
449 the College of Abitibi-Témiscamingue, and the Technology Centre for Industrial Waste (Centre
450 Technologique des Résidus Industriels) through its partners on this project, Airex Energy and
451 Iamgold Corporation. The first author, Dr. Flavia Lega Braghiroli, also sincerely acknowledges
452 NSERC financial support via a Banting Postdoctoral Fellowship (2017–2019). The authors also
453 thank Anne-Marie Marleau Claveau, Félicia Porqueres, Maéva Giasson, Gilles Villeneuve,
454 Mamadou Dia, Nicolas Bergeron and Hélie Jacob Turmel for their assistance with experiments,
455 analysis and testing in the laboratory.

456

457 **References**

- 458 Adebisi, G. A., Chowdhury, Z. Z., & Alaba, P. A. (2017a). Equilibrium, kinetic, and
459 thermodynamic studies of lead ion and zinc ion adsorption from aqueous solution onto
460 activated carbon prepared from palm oil mill effluent. *Journal of Cleaner Production*,
461 *148*, 958–968. doi:10.1016/j.jclepro.2017.02.047
- 462 Adebisi, G. A., Chowdhury, Z. Z., Hamid, S. B. A., & Ali, E. (2017b). Equilibrium isotherm,
463 kinetic, and thermodynamic studies of divalent cation adsorption onto *Calamus*
464 *Gracilis* sawdust-based activated carbon. *BioResources*, *12*(2), 2872–2898.
- 465 Aharoni, C., & Tompkins, F. C. (1970). Kinetics of adsorption and desorption and the Elovich
466 equation. *Advances in Catalysis*, *21*, 1–49. doi:10.1016/S0360-0564(08)60563-5
- 467 Akar, S. T., Akar, T., Kaynak, Z., Anilan, B., Cabuk, A., Tabak, Ö., et al. (2009). Removal of
468 copper(II) ions from synthetic solution and real wastewater by the combined action of
469 dried *Trametes versicolor* cells and montmorillonite. *Hydrometallurgy*, *97*(1–2), 98–
470 104. doi:10.1016/j.hydromet.2009.01.009
- 471 Baccar, R., Bouzid, J., Feki, M., & Montiel, A. (2009). Preparation of activated carbon from
472 Tunisian olive-waste cakes and its application for adsorption of heavy metal ions.
473 *Journal of Hazardous Materials*, *162*(2–3), 1522–1529.
474 doi:10.1016/j.jhazmat.2008.06.041
- 475 Banerjee, S., Mukherjee, S., LaminKa-ot, A., Joshi, S. R., Mandal, T., & Halder, G. (2016).
476 Biosorptive uptake of Fe^{2+} , Cu^{2+} and As^{5+} by activated biochar derived from
477 *Colocasia esculenta*: isotherm, kinetics, thermodynamics, and cost estimation. *Journal*
478 *of Advanced Research*, *7*(5), 597–610. doi:10.1016/j.jare.2016.06.002
- 479 Bilal, M., Shah, J. A., Ashfaq, T., Gardazi, S. M. H., Tahir, A. A., Pervez, A., et al. (2013).
480 Waste biomass adsorbents for copper removal from industrial wastewater—a review.
481 *Journal of Hazardous Materials*, *263*, 322–333. doi:10.1016/j.jhazmat.2013.07.071

482 Bouchelta, C., Medjram, M. S., Zoubida, M., Chekkat, F. A., Ramdane, N., & Bellat, J.-P.
483 (2012). Effects of pyrolysis conditions on the porous structure development of date
484 pits activated carbon. *Journal of Analytical and Applied Pyrolysis*, *94*, 215–222.
485 doi:10.1016/j.jaap.2011.12.014

486 Braghiroli, F. L., Bouafif, H., Hamza, N., Bouslimi, B., Neculita, C. M., & Koubaa, A.
487 (2018a). The influence of pilot-scale pyro-gasification and activation conditions on
488 porosity development in activated biochars. *Biomass and Bioenergy*, *118*, 105–114.
489 doi:10.1016/j.biombioe.2018.08.016

490 Braghiroli, F. L., Bouafif, H., Neculita, C. M., & Koubaa, A. (2018b). Activated biochar as an
491 effective sorbent for organic and inorganic contaminants in water. *Water, Air, Soil*
492 *Pollution*, *229*(7). doi:10.1007/s11270-018-3889-8

493 Brunauer, S., Emmett, P. H., & Teller, E. (1938). Adsorption of gases in multimolecular
494 layers. *Journal of the American Chemical Society*, *60*(2), 309–319.
495 doi:10.1021/ja01269a023

496 Calo, J. M., & Perkins, M. T. (1987). A heterogeneous surface model for the “steady-state”
497 kinetics of the boudouard reaction. *Carbon*, *25*(3), 395–407. doi:10.1016/0008-
498 6223(87)90011-X

499 Chowdhury, Z. Z., Hasan, Md. R., Abd Hamid, S. B., Marlina Samsudin, E., Zain, S. Mohd.,
500 & Khalid, K. (2015). Catalytic pretreatment of biochar residues derived from
501 lignocellulosic feedstock for equilibrium studies of manganese, Mn(II) cations from
502 aqueous solution. *RSC Advances*, *5*(9), 6345–6356. doi:10.1039/C4RA09709B

503 Chowdhury, Z. Z., Zain, S. M., Khan, R. A., Rafique, R. F., & Khalid, K. (2012). Batch and
504 fixed bed adsorption studies of lead (II) cations from aqueous solutions onto granular
505 activated carbon derived from *Mangostana Garcinia* shell. *BioResources*, *7*(3), 2895–
506 2915.

507 Cuppett, J. D. (2006). Evaluation of copper speciation and water quality factors that affect
508 aqueous copper tasting response. *Chemical Senses*, 31(7), 689–697.
509 doi:10.1093/chemse/bjl010

510 Ding, Z., Hu, X., Wan, Y., Wang, S., & Gao, B. (2016). Removal of lead, copper, cadmium,
511 zinc, and nickel from aqueous solutions by alkali-modified biochar: batch and column
512 tests. *Journal of Industrial and Engineering Chemistry*, 33, 239–245.
513 doi:10.1016/j.jiec.2015.10.007

514 Dubinin, M. M. (1989). Fundamentals of the theory of adsorption in micropores of carbon
515 adsorbents: Characteristics of their adsorption properties and microporous structures.
516 *Carbon*, 27(3), 457–467. doi:10.1016/0008-6223(89)90078-X

517 Dudka, S., & Adriano, D. C. (1997). Environmental impacts of metal ore mining and
518 processing: a review. *Journal of Environment Quality*, 26(3), 590.
519 doi:10.2134/jeq1997.00472425002600030003x

520 Environment and Climate Change Canada. (1999). Environmental Code of Practice for Base
521 Metals Smelters and Refineries: Code of Practice, Canadian Environmental Protection
522 Act. Available at [http://ec.gc.ca/lcpe-cepa/default.asp?lang=En&n=9233A7E7-](http://ec.gc.ca/lcpe-cepa/default.asp?lang=En&n=9233A7E7-1&offset=2)
523 [1&offset=2](http://ec.gc.ca/lcpe-cepa/default.asp?lang=En&n=9233A7E7-1&offset=2). Accessed 15 June 2018

524 Freundlich, H. M. F. (1906). Over the adsorption in solution. *The Journal of Physical*
525 *Chemistry*, 57, 385–471.

526 Gregg, S. J., & Sing, K. S. W. (1991). *Adsorption, surface area, and porosity*. London, UK:
527 Academic Press.

528 Hamid, S. B. A., Chowdhury, Z. Z., & Zain, S. M. (2014). Base catalytic approach: a
529 promising technique for the activation of biochar for equilibrium sorption studies of
530 copper, Cu(II) ions in single solute system. *Materials*, 7(4), 2815–2832.
531 doi:10.3390/ma7042815

532 Health Canada. (1992). Guidelines for Canadian Drinking Water Quality: Guideline Technical
533 Document – Copper. Available at [https://www.canada.ca/content/dam/canada/health-
canada/migration/healthy-canadians/publications/healthy-living-vie-saine/water-
copper-cuivre-eau/alt/water-copper-cuivre-eau-eng.pdf](https://www.canada.ca/content/dam/canada/health-
534 canada/migration/healthy-canadians/publications/healthy-living-vie-saine/water-
535 copper-cuivre-eau/alt/water-copper-cuivre-eau-eng.pdf). Accessed 15 June 2018

536 Kołodyńska, D., Krukowska, J., & Thomas, P. (2017). Comparison of sorption and desorption
537 studies of heavy metal ions from biochar and commercial active carbon. *Chemical
538 Engineering Journal*, 307, 353–363. doi:10.1016/j.cej.2016.08.088

539 Lagergren, S. (1898). About the theory of so-called adsorption of soluble substances. *Kungl.
540 Svenska vetenskapsakademiens handlingar*, 24(4), 1–39.

541 Lamb, D. T., Naidu, R., Ming, H., & Megharaj, M. (2012). Copper phytotoxicity in native and
542 agronomical plant species. *Ecotoxicology and Environmental Safety*, 85, 23–29.
543 doi:10.1016/j.ecoenv.2012.08.018

544 Langmuir, I. (1918). The adsorption of gases on plane surfaces of glass, mica and platinum.
545 *Journal of the American Chemical Society*, 40(9), 1361–1403.
546 doi:10.1021/ja02242a004

547 Lazzarini, A., Piovano, A., Pellegrini, R., Leofanti, G., Agostini, G., Rudić, S., et al. (2016). A
548 comprehensive approach to investigate the structural and surface properties of
549 activated carbons and related Pd-based catalysts. *Catalysis Science & Technology*,
550 6(13), 4910–4922. doi:10.1039/C6CY00159A

551 Lee, J. A., Marsden, I. D., & Glover, C. N. (2010). The influence of salinity on copper
552 accumulation and its toxic effects in estuarine animals with differing osmoregulatory
553 strategies. *Aquatic Toxicology*, 99(1), 65–72. doi:10.1016/j.aquatox.2010.04.006

554 Lehmann, J., & Joseph, S. (Eds.). (2015). *Biochar for Environmental Management: Science,
555 Technology and Implementation*. Abingdon, UK: Routledge.

556 Lima, I. M., Boateng, A. A., & Klasson, K. T. (2010). Physicochemical and adsorptive
557 properties of fast-pyrolysis bio-chars and their steam activated counterparts. *Journal of*
558 *Chemical Technology & Biotechnology*, 85, 1515–1521. doi:10.1002/jctb.2461

559 Lima, I. M., Boykin, D. L., Thomas Klasson, K., & Uchimiya, M. (2014). Influence of post-
560 treatment strategies on the properties of activated chars from broiler manure.
561 *Chemosphere*, 95, 96–104. doi:10.1016/j.chemosphere.2013.08.027

562 Liu, W.-J., Jiang, H., & Yu, H.-Q. (2015). Development of biochar-based functional materials:
563 toward a sustainable platform carbon material. *Chemical Reviews*, 115(22), 12251–
564 12285. doi:10.1021/acs.chemrev.5b00195

565 Marsh, H., & Rodríguez-Reinoso, F. (2006). *Activated carbon* (1st ed.). Amsterdam, NL:
566 Elsevier.

567 Mohan, D., & Chander, S. (2001). Single component and multi-component adsorption of metal
568 ions by activated carbons. *Colloids and Surfaces A: Physicochemical and Engineering*
569 *Aspects*, 177(2–3), 183–196. doi:10.1016/S0927-7757(00)00670-1

570 Mohan, Dinesh, & Chander, S. (2006). Removal and recovery of metal ions from acid mine
571 drainage using lignite—a low cost sorbent. *Journal of Hazardous Materials*, 137(3),
572 1545–1553. doi:10.1016/j.jhazmat.2006.04.053

573 Nordstrom, D. K., Blowes, D. W., & Ptacek, C. J. (2015). Hydrogeochemistry and
574 microbiology of mine drainage: an update. *Environmental Geochemistry of Modern*
575 *Mining*, 57, 3–16. doi:10.1016/j.apgeochem.2015.02.008

576 Peng, H., Gao, P., Chu, G., Pan, B., Peng, J., & Xing, B. (2017). Enhanced adsorption of
577 Cu(II) and Cd(II) by phosphoric acid-modified biochars. *Environmental Pollution*,
578 229, 846–853. doi:10.1016/j.envpol.2017.07.004

579 Radovic, L. R., & Rodriguez-Reinoso, F. (1997). In P. A. Thrower (Ed.), *Chemistry and*
580 *Physics of Carbon* (Vol. 25). New York, USA: Marcel Dekker.

581 Ríos, C. A., Williams, C. D., & Roberts, C. L. (2008). Removal of heavy metals from acid
582 mine drainage (AMD) using coal fly ash, natural clinker and synthetic zeolites.
583 *Journal of Hazardous Materials*, 156(1–3), 23–35. doi:10.1016/j.jhazmat.2007.11.123

584 Sekhula, M. M., Okonkwo, J. O., Zvinowanda, C. M., Agyei, N. N., & Chaudhary, A. J.
585 (2012). Fixed bed column adsorption of Cu (II) onto maize tassel-PVA beads. *Journal*
586 *of Chemical Engineering & Process Technology*, 03(02). doi:10.4172/2157-
587 7048.1000131

588 Shim, T., Yoo, J., Ryu, C., Park, Y.-K., & Jung, J. (2015). Effect of steam activation of
589 biochar produced from a giant *Miscanthus* on copper sorption and toxicity.
590 *Bioresource Technology*, 197, 85–90. doi:10.1016/j.biortech.2015.08.055

591 Sing, K. S. W. (1985). Reporting physisorption data for gas/solid systems with special
592 reference to the determination of surface area and porosity (Recommendations 1984).
593 *Pure and Applied Chemistry*, 57(4), 603–619. doi:10.1351/pac198557040603

594 Tan, X., Liu, S., Liu, Y., Gu, Y., Zeng, G., Hu, X., et al. (2017). Biochar as potential
595 sustainable precursors for activated carbon production: multiple applications in
596 environmental protection and energy storage. *Bioresource Technology*, 227, 359–372.
597 doi:10.1016/j.biortech.2016.12.083

598 Tarazona, P. (1995). Solid-fluid transition and interfaces with density functional approaches.
599 *Proceedings of the 14th European Conference on Surface Science*, 331, 989–994.
600 doi:10.1016/0039-6028(95)00170-0

601 Visual MINTEQ version 3.1. (2018). <https://vminteq.lwr.kth.se/>.

602 Wilson, K., Yang, H., Seo, C. W., & Marshall, W. E. (2006). Select metal adsorption by
603 activated carbon made from peanut shells. *Bioresource Technology*, 97(18), 2266–
604 2270. doi:10.1016/j.biortech.2005.10.043

605 Wu, F.-C., Tseng, R.-L., & Juang, R.-S. (2009). Characteristics of Elovich equation used for
606 the analysis of adsorption kinetics in dye-chitosan systems. *Chemical Engineering*
607 *Journal*, 150(2–3), 366–373. doi:10.1016/j.ccej.2009.01.014

608 Xie, R., Jin, Y., Chen, Y., & Jiang, W. (2017). The importance of surface functional groups in
609 the adsorption of copper onto walnut shell derived activated carbon. *Water Science*
610 *and Technology*, 76(11), 3022–3034. doi:10.2166/wst.2017.471

611
612

613

614

615

616

617

618

619

620

621

622

623

624

625

626

627

628

629

630

631 **Table captions**

632 **Table 1.** Textural and physicochemical properties of biochars and activated biochars

633 **Table 2.** Kinetic parameters obtained from the adsorption of Cu onto biochars and activated
634 biochars

635 **Table 3.** Parameters of Cu adsorption isotherms onto biochars and activated biochars

636 **Table 4.** Comparative sorption capacity of activated biochars and commercial activated carbon
637 for Cu²⁺ in water

638 **Table 5.** Composition (mg L⁻¹, except for pH and Eh) of initial and final (after adsorption with
639 KOHBBS) AMD

640

641

642

643

644

645

646

647

648

649

650

651

652

653

654

655

656 **Figure captions**

657 **Fig. 1.** SEM images of activated biochars prepared from WB and BS wood residues in presence
658 of CO₂ (a and b); steam (c and d); and KOH (e and f)

659 **Fig. 2.** Adsorbed amounts of Cu²⁺ at initial concentration of 100 mg L⁻¹ (q_t) as function of time
660 for both biochars: () BWB, () BBS; and activated biochars: (Δ) CO₂BWB, (▲)
661 CO₂BBS, (○) H₂O BWB, (●) H₂O BBS, (□) KOH BWB, and (■) KOH BBS

662 **Fig. 3.** a) Adsorbed isotherms of Cu²⁺, and b) Cu²⁺ adsorption (%) as function of different initial
663 concentrations of Cu²⁺ (C₀ = 5, 10, 20, 50, 100, and 200 mg L⁻¹) for both biochars: ()
664 BWB, () BBS; and activated biochars: () CO₂BWB, (Δ) CO₂BBS, (▲) H₂O BWB, (○)
665 H₂O BBS, (●) KOH BWB, (□) and () KOH BBS ■

666 **Fig. 4.** Adsorbed Cu²⁺ from real effluent (mg L⁻¹) as function of the contact time for both
667 biochars: (◇) BWB, (◆) BBS; and activated biochars: (Δ) CO₂BWB, (▲) CO₂BBS, (○)
668 H₂O BWB, (●) H₂O BBS, (□) KOH BWB, and (■) KOH BBS

669 **Fig. 5.** Desorption efficiency of Cu²⁺ ions after a) chemical regeneration using three different
670 eluents: HNO₃ 0.1 M, H₂SO₄ 0.5 M, and HCl 1 M, and b) after six cycles adsorption-
671 desorption

672

673

674

675

676

677

678

679

680 **Table 1.** Textural and physicochemical properties of biochars and activated biochars

| | <i>BWB</i> | <i>BBS</i> | <i>CO2BWB</i> | <i>CO2BBS</i> | <i>H2OBWB</i> | <i>H2OBBS</i> | <i>KOHBWB</i> | <i>KOHBBS</i> |
|---|------------|------------|---------------|---------------|---------------|---------------|---------------|---------------|
| <i>Textural properties</i> | | | | | | | | |
| S _{BET} (m ² g ⁻¹) | 177* | 208* | 881** | 735** | 590** | 412** | 1700** | 1662** |
| V _t (cm ³ g ⁻¹) | | | 0.53 | 0.39 | 0.34 | 0.18 | 0.75 | 0.72 |
| V _{μ, N₂} (cm ³ g ⁻¹) | | | 0.33 | 0.28 | 0.23 | 0.17 | 0.75 | 0.72 |
| V _{μ, CO₂} (cm ³ g ⁻¹) | 0.11 | 0.14 | 0.28 | 0.20 | 0.22 | 0.20 | 0.36 | 0.45 |
| V _m (cm ³ g ⁻¹) | | | 0.20 | 0.11 | 0.11 | 0.01 | 0.00 | 0.00 |
| <i>Physicochemical properties</i> | | | | | | | | |
| pH | 5.0 | 6.7 | 10.2 | 10.3 | 9.9 | 9.3 | 8.2 | 9.3 |
| C (%) | 75.4 | 75.4 | 89.9 | 88.9 | 89.1 | 83.8 | 77.5 | 80.1 |
| H (%) | 3.5 | 3.8 | 0.9 | 0.6 | 0.6 | 0.8 | 1.7 | 1.0 |
| N (%) | 0.9 | 0.9 | 0.4 | 1.2 | 0.2 | 0.8 | 2.0 | 2.7 |
| S (%) | 0.5 | 0.5 | 0.0 | 0.1 | 0.0 | 0.0 | 0.1 | 0.0 |
| O° (%) | 19.7 | 19.4 | 8.8 | 9.2 | 10.1 | 14.6 | 18.7 | 16.2 |

681 S_{BET} obtained from *CO₂ and **N₂ adsorption analysis; °O content was obtained by difference (O% = 100 – CHNS%)

682

683

684

685

686

687

688

689

690

691

692

693

694 **Table 2.** Kinetic parameters obtained from the adsorption of Cu onto biochars and activated
 695 biochars

| | <i>Pseudo-first order</i> | | | | <i>Pseudo-second order</i> | | | <i>Elovich's equation</i> | | |
|--------|-------------------------------------|--------------------------------|-----------------------------|-------|--------------------------------|------------------------------------|-------|----------------------------------|--------------------------------|-------|
| | $q_{exp.}$ (mg g ⁻¹) | q_e (mg g ⁻¹) | k_1 (h ⁻¹) | R^2 | q_e (mg g ⁻¹) | k_2 (mg (g h) ⁻¹) | R^2 | a (mg (g h) ⁻¹) | $1/b$ (mg g ⁻¹) | R^2 |
| BWB | 10.04 | 9.09 | 0.04 | 0.79 | 4.78 | 0.0041 | 0.65 | 2.79 | 2.43 | 0.82 |
| BBS | 9.98 | 10.81 | 0.05 | 0.99 | 14.14 | 0.0093 | 0.72 | 2.22 | 2.06 | 0.97 |
| CO2BWB | 48.91 | 33.99 | 0.081 | 0.92 | 35.71 | 0.0049 | 0.51 | 2.17 . 10 ¹ | 11.51 | 0.92 |
| CO2BBS | 25.25 | 23.96 | 0.072 | 0.83 | 11.4 | 0.0018 | 0.33 | 1.13 . 10 ⁴ | 2.04 | 0.96 |
| H2OBWB | 24.90 | 8.86 | 0.058 | 0.61 | 10.16 | 0.0029 | 0.27 | 2.07 . 10 ¹ | 4.55 | 0.95 |
| H2OBBS | 19.18 | 7.95 | 0.061 | 0.56 | 3.80 | 0.024 | 0.12 | 7.83 | 4.90 | 0.67 |
| KOBBW | 25.15 | 9.08 | 0.069 | 0.66 | 7.40 | 0.0132 | 0.06 | 1.08 . 10 ³ | 2.70 | 0.73 |
| KOHBBS | 36.71 | 7.61 | 0.053 | 0.70 | 9.51 | 0.0023 | 0.02 | 9.79 . 10 ² | 4.07 | 0.95 |

696

697

698

699

700

701

702

703

704

705

706

707

708

709

710

711

712 **Table 3.** Parameters of Cu adsorption isotherms onto biochars and activated biochars

| | <i>Freundlich</i> | | | <i>Langmuir</i> | | | | |
|--------|-------------------|------|-------|---------------------------------|---------------------------------|---------------------------|-----------|-------|
| | k_f | n | R^2 | q_{exp} (mg g ⁻¹) | q_{max} (mg g ⁻¹) | b (L mg ⁻¹) | R_L | R^2 |
| BWB | 1.16 | 0.52 | 0.82 | 85 | 120 | 0.001 | 0.45–0.99 | 0.15 |
| BBS | 1.45 | 0.60 | 0.88 | 77 | 105 | 0.001 | 0.45–0.99 | 0.21 |
| CO2BWB | 17.66 | 0.26 | 0.90 | 127 | 127 | 0.016 | 0.06–0.93 | 0.92 |
| CO2BBS | 5.82 | 0.34 | 0.89 | 98 | 102 | 0.005 | 0.16–0.98 | 0.73 |
| H2OBWB | 11.11 | 0.26 | 0.80 | 122 | 132 | 0.005 | 0.15–0.97 | 0.77 |
| H2OBBS | 5.45 | 0.30 | 0.77 | 101 | 100 | 0.003 | 0.22–0.98 | 0.51 |
| KOBBWB | 10.80 | 0.26 | 0.86 | 105 | 109 | 0.006 | 0.14–0.97 | 0.73 |
| KOHBBS | 17.51 | 0.23 | 0.94 | 137 | 132 | 0.009 | 0.10–0.96 | 0.81 |

713
714
715
716
717
718
719
720
721
722
723
724
725
726
727
728
729
730
731
732
733

734 **Table 4.** Comparative sorption capacity of activated biochars and commercial activated carbon
 735 for Cu²⁺ in water

| <i>Activated biochar precursor</i> | <i>gAC:mL</i> | <i>pH</i> | <i>Activation/ S_{BET} (m² g⁻¹)</i> | <i>q_{max} (mg g⁻¹)</i> | <i>Kinetic/ Isotherm model</i> | <i>C₀ (mg L⁻¹)</i> | <i>References</i> |
|------------------------------------|---------------|-----------|---|--|--|--|-------------------------|
| Soybean straw | 1:100 | 4.8 | Steam (up to 793) | 96% removal | – | 64 | (Lima et al. 2010) |
| Date pits | 0.1:100 | – | Steam (1467) | 203 | Langmuir | 600 | (Bouchelta et al. 2012) |
| Waste peels of mangosteen fruits | 0.4:100 | 5.5 | CO ₂ /KOH (367) | 19 | Pseudo-second order; Langmuir and Freundlich | 50–100 | (Hamid et al. 2014) |
| Broiler litter Broiler cake | 1:100 | 4.8 | Steam (up to 425) | 104 49 | – | 2690 | (Lima et al. 2014) |
| <i>Miscanthus</i> plant | 0.2:100 | 6 | Steam (322) | 14 | Two-compartment model; Langmuir | 0.2–150 | (Shim et al. 2015) |
| <i>Colocasia esculenta</i> roots | 0.06:100 | 5 | Steam (102) | 2.3 | Pseudo-second order; Langmuir | 30 | (Banerjee et al. 2016) |
| Hickory chips | – | 5 | NaOH (873) | 54 | – | 2–250 | (Ding et al. 2016) |
| Pine sawdust | 0.025:100 | 4.5 | H ₃ PO ₄ (900) | 2 | Freundlich | 1–10 | (Peng et al. 2017) |
| White birch | 0.1:100 | 4.5 | CO ₂ (880) | 127 | Elovich, Freundlich | 5–1000 | Present study |
| Black spruce | 0.1:100 | 4.5 | KOH (1662) | 137 | Elovich, Freundlich | 5–1000 | Present study |
| NORIT C GRAN | 1:100 | 4.8 | H ₃ PO ₄ (624) | 56 | - | 1270 | (Wilson et al. 2006) |

736
 737
 738
 739
 740
 741
 742
 743
 744
 745
 746
 747
 748
 749
 750
 751

752 **Table 5.** Composition (mg L⁻¹, except for pH and Eh) of initial and final (after adsorption with
 753 KOHBBS) AMD

| <i>Parameter</i> | <i>Initial AMD</i> | <i>Final AMD</i> | <i>Removal (%)</i> |
|-------------------------------|------------------------|----------------------|------------------------|
| pH | 2.70 | 2.60 | - |
| Eh (mV) | 584 | 548 | - |
| Dissolved oxygen | 10.0 | 7.90 | - |
| Al | 141 | 145 | 0 |
| Ca | 466 | 468 | 0 |
| Cd | < 0.05 | < 0.05 | 0 |
| Co | 9.38 | 0.502 | 95 |
| Cr | 0.067 | 0.093 | 0 |
| Cu | 1.753 | 0.0055 | 99 |
| Fe | 468 | 405 | 13 |
| K | 4.41 | 24.9 | 0 |
| Mg | 131 | 138 | 0 |
| Mn | 10.9 | 9.72 | 11 |
| Na | 57 | 52.5 | 8 |
| Ni | 0.367 | 0.605 | 0 |
| Pb | 0.143 | 0.0813 | 43 |
| Zn | 4.92 | 4.62 | 6 |
| NO ₂ ⁻ | 16 | 16.3 | 0 |
| NO ₃ ⁻ | 750 | 726 | 3 |
| SO ₄ ²⁻ | 2390 | 2411 | - |
| PO ₄ ³⁻ | 16.1 | 12.1 | 25 |

754

755